BIOCHEMISTRY
including biophysical chemistry & molecular biology

Article

pubs.acs.org/biochemistry

Femtosecond Dynamics of Short-Range Protein Electron Transfer in Flavodoxin

Ting-Fang He, Lijun Guo, Xunmin Guo, Chih-Wei Chang, Lijuan Wang, and Dongping Zhong*

Department of Physics, Department of Chemistry and Biochemistry, and Programs of Biophysics, Chemical Physics, and Biochemistry, The Ohio State University, Columbus, Ohio 43210, United States

ABSTRACT: Intraprotein electron transfer (ET) in flavoproteins is important for understanding the correlation of their redox, configuration, and reactivity at the active site. Here, we used oxidized flavodoxin as a model system and report our complete characterization of a photoinduced redox cycle from the initial charge separation in 135−340 fs to subsequent charge recombination in 0.95−1.6 ps and to the final cooling relaxation of the product(s) in 2.5−4.3 ps. With 11 mutations at the active site, we observed that these ultrafast ET dynamics, much faster than active-site relaxation, mainly depend on the reduction potentials of the electron donors with minor changes caused by mutations, reflecting a highly localized ET reaction between the stacked donor and acceptor at a van der Waals distance and leading to a gas-phase type of bimolecular ET reaction confined in the active-site nanospace. Significantly, these ultrafast ET reactions ensure our direct observation of vibrationally excited reaction product(s), suggesting that the back ET barrier is effectively reduced because of the decrease in the total free energy in the Marcus inverted region, leading to the accelerated charge recombination. Such vibrationally coupled charge recombination should be a general feature of flavoproteins with similar configurations and interactions between the cofactor flavin and neighboring aromatic residues.

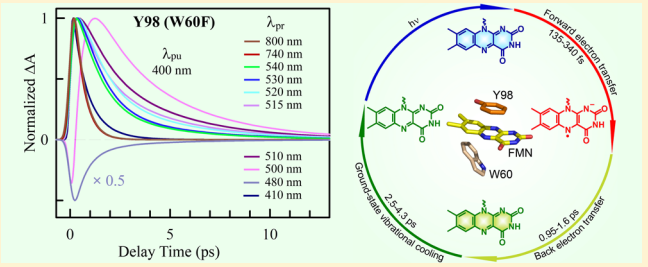

Electron transfer (ET) is ubiquitous in biology and essential to a variety of biological activities such as converting chemical energy,[1,2] catalyzing enzymatic reactions,[3−5] and triggering biological signaling.[6,7] To understand ET dynamical behaviors in proteins, for the past several decades, various experiments examining long-range (>10 Å) ET have been designed and conducted,[8−11] and theoretical models[12−15] were developed to elucidate the relationship between ET rates and donor−acceptor distance (r) or electronic coupling constant (J), driving force ($\Delta G°$), and reorganization energy (λ). Typically, these ET dynamics occur on time scales of nanoseconds or longer, and the systems are in equilibrium with local environments. These experimental observations can basically be understood on the basis of the original Marcus theory in the normal ($-\Delta G° \leq \lambda$) or inverted region ($-\Delta G° > \lambda$). However, when the donor−acceptor separation is <10 Å, the ET dynamics can occur ultrafast in the range of femtoseconds to hundreds of picoseconds, a time scale that is similar to the time scales of local environment relaxation of the solvent and protein.[2−5] Thus, the ET dynamics are in nonequilibrium, and the processes follow nonexponential dynamical behaviors.[3,4,16] Usually, the extended Sumi−Marcus two-dimensional model[17] with quantum correction[18] can be used to simulate experimental results, providing molecular insights into short-range protein ET. The vibrational modes could be observed to greatly enhance ET dynamics in chemical systems,[18,19] effectively reducing the ET barrier, but such a vibrational quantum effect has not been directly observed in protein ET. A theoretical study was recently proposed to explain the direct coupling of two low-frequency vibrational modes to charge separation in bacterial photosynthetic reaction centers.[20]

Furthermore, when the donor and acceptor are in the proximity of each other, for instance, in van der Waals contact, the short-range ET dynamics in proteins could be even faster than the local relaxation, leading to a "frozen" protein environment with a heterogeneous distribution of electrostatics. In this case, although the energetics is related to the local electrostatics, the ET reaction is relatively "isolated" and would be a confined bimolecular reaction. In this report, as part of our enduring efforts[16,21] to elucidate the molecular mechanism of ultrafast nonequilibrium protein ET in the short range, we report our careful characterization of the ET dynamics in a model system of *Desulfovibrio vulgaris* flavodoxin.

Flavodoxin belongs to one class of flavoproteins and functions as an electron shuttle through the cofactor of flavin mononucleotide (FMN).[22] Structurally, flavodoxin consists of five parallel β-strands surrounded by several α-helices as shown in Figure 1 (left). The prosthetic FMN group is noncovalently but tightly bound by a series of interactions with protein residues.[23] One of the key interactions is the $\pi-\pi$ stacking of the isoalloxazine ring with Y98 and W60 via van der Waals contacts (Figure 1, right) to form a sandwich configuration. Such recognition of FMN excludes water from the binding

Received: August 19, 2013
Revised: November 29, 2013
Published: November 30, 2013

   dx.doi.org/10.1021/bi401137u | *Biochemistry* 2013, 52, 9120−9128

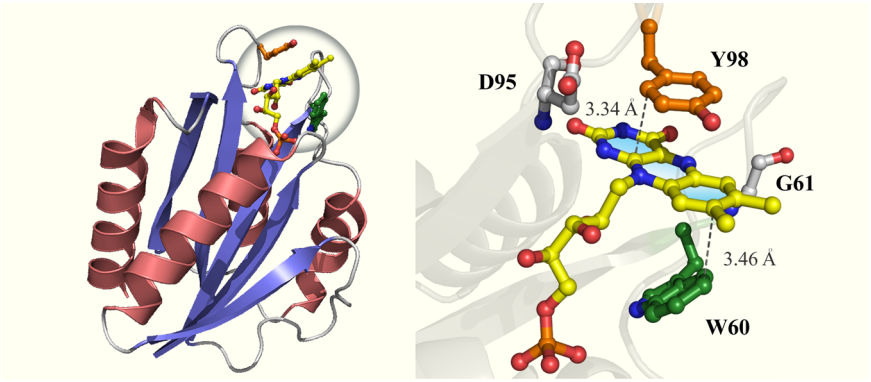

Figure 1. X-ray crystallographic structure (left) of oxidized *D. vulgaris* flavodoxin (Protein Data Bank entry 2FX2). Close-up view (right) of the local configuration at the FMN-binding site. The FMN cofactor (yellow) is sandwiched between two neighboring aromatic residues W60 (green) and Y98 (orange) are in van der Waals contact. Also shown are acidic residue D95 and the backbone carbonyl group of G61 in the proximity of FMN.

Table 1. Time Scales of ET and Subsequent Cooling Dynamics and Related Energies[a]

	mutant	donor	τ_{FET}[b]	τ_{FET}[c]	τ_{BET}[d]	$\tau_{cooling}$	$E_{m,7}$(FMN/FMNH)[e]	$\Delta G°_{FET}$[f]	$\Delta G°_{BET}$[f]
i	W60A[g]	Y98	0.34	0.49	0.95	3.7–4.0	−0.16	−0.66	−1.84
	W60F	Y98	0.30	0.49	0.95	3.7–4.0			
ii	Y98F	W60	0.26	0.37	1.61	3.3–3.8	−0.15	−0.99	−1.50
	Y98A	W60	0.25	0.37	1.00	2.5–3.5	−0.19	−0.95	−1.54
	Y98H	W60	0.20	0.32	1.43	3.2–4.2	−0.19	−0.96	−1.54
	Y98R	W60	0.19	0.32	1.10	2.6–3.6	−0.17	−0.98	−1.51
iii	W60Y	Y60, Y98	0.26	0.46	0.95	3.7–4.0			
	Y98W	W60, W98			1.10	3.0–4.0	−0.15		
iv	WT	W60, Y98	0.16	0.18	1.56, 0.95	3.0–4.3	−0.15		
	G61V	W60, Y98	0.15	0.16	1.23, 0.95	3.0–3.5	−0.33		
	G61A	W60, Y98	0.15	0.16	1.23, 0.95	3.0–3.5	−0.26		
	D95N	W60, Y98	0.14	0.18	1.51, 0.95	3.0–4.0	−0.15		

[a]All times in picoseconds and energies in electronvolts. [b]From fluorescence detection. [c]From transient absorption detection. [d]For the dual donors of W and Y, the first column for W and the second for Y. [e]These data are from refs 29, 31, 41, and 42. E(FMN/FMN$^-$) could be calculated from $E_{m,7}$(FMN/FMNH) + 0.06 × log[(1 + [H$^+$]/K_{ox})(1 + [H$^+$]/K_{red})] with known values of 10^{-7} for [H$^+$], 1 for K_{ox}, and $10^{-10.5}$ for K_{red}. [f]The free energies were not calculated for the dual donors and could be separately estimated for W and Y as for the single donor with $E_{m,7}$. [g]There is another minor component with 1.82 ps and 4% amplitude in the FET determined by fluorescence detection.

pocket, and only the partial *o*-xylene ring is exposed to surface hydration water molecules. We have recently characterized the dynamics of the active-site solvation in three redox states (FMN, FMNH$^•$, and FMNH$^-$) via site-directed mutagenesis to replace the electron donors of Y98 and W60 with the inert aromatic residue F (double mutant W60F/Y98F).[24] The local relaxation was observed to occur over a wide time scale from a few picoseconds to tens to hundreds of picoseconds. With well-characterized active-site relaxation dynamics, we can quantitatively examine the short-range nonequilibrium ET dynamics in flavodoxin.

We report here the characterization of both forward and backward ET in the complete photoinduced redox cycle of oxidized FMN. Although the ET dynamics have been reported in several flavoproteins,[25−28] including flavodoxin,[28] the majority of studies examined only the forward ET dynamics. These studies showed that the intraprotein ET can occur over a wide time scale from hundreds of femtoseconds to tens of picoseconds. Here, with site-specific mutation and femtosecond resolution, we systematically studied 11 mutants to evaluate the short-range ET dynamics with different redox energies, including two mutations of neighboring residues of G61 and D95 that have been shown to strongly affect the redox states of FMN.[29,30] These 11 mutants and the wild type (WT) are classified into four groups in Table 1 (also see Figure 1, right): (i) Y98 as the only ET donor with mutations W60F and W60A, (ii) W60 as the only ET donor with mutations Y98F, Y98A, Y98H, and Y98R, (iii) two similar ET donors of Y60/Y98 and W60/W98 with mutations W60Y and Y98W, respectively, and (iv) both W60 and Y98 as the ET donors with the wild type and G61A, G61V, and D95N mutants. By extensively characterizing the ET dynamics for 12 proteins, we observed ultrafast nonequilibrium ET dynamics in both forward (FET) and backward (BET) directions, modulated by different redox potentials. More significantly, we directly observed the vibrationally involved BET process and subsequent vibrational cooling dynamics of the product(s) at the active site of the protein.

■ MATERIALS AND METHODS

Protein Preparation. The purification procedures for flavodoxin and the mutants have been well established.[31,32] For femtosecond-resolved experiments, the flavodoxin was prepared at concentrations of 60−250 μM in a 50 mM phosphate buffer solution (pH 7). To remove the unbound FMN molecule, the sample was passed through a mini-desalting column (Sephadex G-25 medium) right before being used. During laser experiments, the sample was under aerobic conditions at room temperature (22 °C).

dx.doi.org/10.1021/bi401137u | *Biochemistry* 2013, 52, 9120−9128

Femtosecond Methods. Femtosecond-resolved measurements were taken using the fluorescence upconversion and transient absorption methods. The experimental layout has been described previously.[33] Briefly, the pump pulse was set at 400 nm with the energy attenuated to ≈100 nJ before it was focused into the sample cell. For the fluorescence upconversion experiments, the fluorescence emission at 538 nm was gated by another 800 nm laser beam in a 0.5 mm thick β-barium borate crystal (BBO, type I). For the transient absorption experiments, the probe pulses at the desired wavelengths between 410 and 800 nm were generated via two optical parametric amplifiers (OPA-800C and TOPAS, Spectra-Physics). The instrument responses are 250−300 and 160−300 fs for fluorescence and transient absorption detection, respectively. All experiments were conducted at the magic angle (54.7°). To prevent heating and photobleaching, the sample was kept in stirring quartz cells with a 1 or 5 mm thickness during laser irradiation.

RESULTS AND DISCUSSION

Reaction Schemes and Probing Strategies. For 12 proteins with four different groups of ET reactions, we can summarize the kinetics as follows: For cases i and ii, the

$$FMN^* + \begin{matrix} Y \\ FET \\ W \end{matrix} \begin{matrix} \xrightarrow{k_1} \\ \xleftarrow{k_2} \end{matrix} FMN^- + \begin{matrix} Y^+ \\ BET \\ W^+ \end{matrix} \begin{matrix} \xrightarrow{k_3} \\ \xleftarrow{k_4} \end{matrix} FMN^\dagger + \begin{matrix} Y \\ W \end{matrix} \xrightarrow[\text{cooling}]{k_5} FMN + \begin{matrix} Y \\ W \end{matrix} \quad [1]\ [2]$$

proteins contain only one ET donor, and thus, the ET dynamics correspond to reactions 1 and 2, respectively. For cases iii and iv, both reactions 1 and 2 occur, but for the former, the two donors are either the same Y or W in the reactions. In Figure 2, we show all the absorption spectra of various species involved in the reactions in the visible region. Figure 2B shows the special absorption spectrum of mutant Y98W and the usual absorption profile of the wild-type (WT) protein and 10 other mutants with the peaks of $S_1 \leftarrow S_0$ (450 nm) and $S_2 \leftarrow S_0$ (380 nm) transitions of FMN in the binding pocket. For Y98W, the absorption extends beyond 650 nm, and this tail suggests the charge transfer character due to electronic delocalization of FMN through stacking with the two aromatic tryptophan residues, W60 and W98.[31] If the high-frequency vibrational modes are involved in the BET reactions and thus enhance the BET rates, the formed hot $FMN^\dagger$ product could be detected at the red edge of the ground-state absorption (inset of Figure 2B). To directly observe such a vibrational effect, i.e., the formation of $FMN^\dagger$ product, the ET reaction rates, k_1 and k_3 in eq 1 or k_2 and k_4 in eq 2, must be faster than the cooling relaxation rate (k_5). Otherwise, $FMN^\dagger$ could not accumulate because of the rate-determining slow ET dynamics. Thus, we need to resolve all elementary steps by monitoring the dynamics of each intermediate involved in the reactions. Figure 2A shows the normalized absorption spectra of three intermediate radicals and excited FMN.[34−36] We can tune different wavelengths to follow the whole dynamics of reactants (FMN*), intermediates ($FMN^{\bullet-}$, W^+, and Y^+), and products ($FMN^\dagger$ and FMN) and thus map out the entire redox cycle and hot vibrational cooling, if any, in the protein.

Femtosecond Charge Separation, Frozen Active-Site Configuration, and Critical Free Energies. Figure 3 shows the typical fluorescence transients gated at the emission peak (538 nm) for the WT and several mutants. Except for the mutant of Y98W, for all 11 other proteins, the fluorescence transients show the dynamics in 135−340 fs. We did not

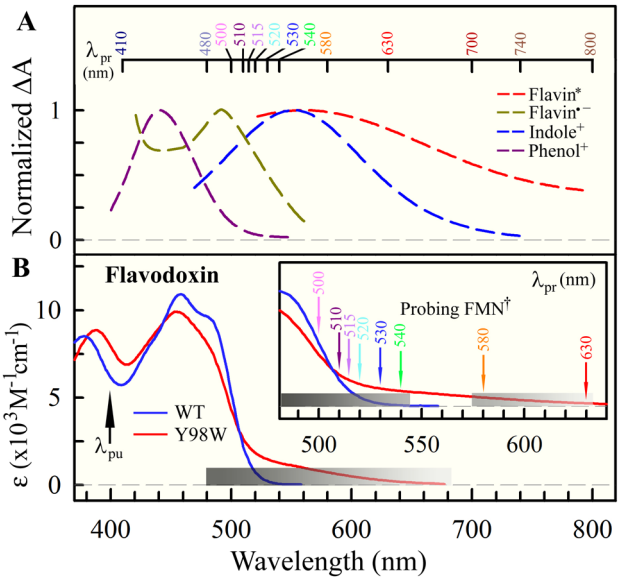

Figure 2. (A) Normalized (transient) absorption spectra of protein-bound FMN* (red) and anionic flavin semiquinone (dark yellow) and free cationic radicals of indole (blue) and phenol (dark purple) in organic solvents. The profile of the phenol radical cation was extracted by direct subtraction of long-lived phenoxyl radical absorption from the mixed spectrum.[34] The various probe wavelengths for the transient absorption experiments are marked at the top. (B) Steady-state absorption spectra of wild-type (blue) and mutant Y98W (red) flavodoxin. The pump wavelength at 400 nm and multiple probe wavelengths (inset) for probing the vibrationally hot FMN molecules are marked by a series of arrows.

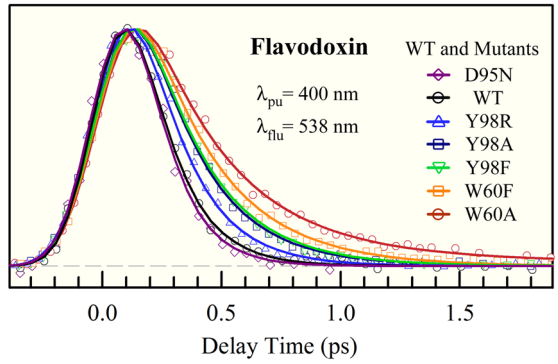

Figure 3. Normalized femtosecond-resolved fluorescence transients of FMN* in flavodoxin mutants gated at 538 nm. Note that in some transients a small long lifetime component (1−2%) due to the presence of a free FMN molecule was removed for the sake of clarity.

observe any fluorescence dynamics for Y98W because of the nature of charge transfer excitation. Except for W60A, all other 10 fluorescence transients show a single-exponential decay behavior. Specifically, for case i, we obtained a value of 302 fs for W60F. For case ii, we obtained values of 258, 247, 204, and 193 fs for Y98F, Y98A, Y98H, and Y98R, respectively. For case iii, we obtained a value of 258 fs for W60Y. For case iv, we obtained values of 157, 154, 149, and 135 fs for the wild type, G61V, G61A, and D95N, respectively. For W60A, we can fit a double-exponential decay in 340 fs with an amplitude of 96% and 1.82 ps (4%) or a stretched exponential decay with 345 fs and a stretched parameter of 0.9.[3−5] These results are listed in Table 1. We noticed that the W60A mutant is less stable than W60F because aromatic residue W60 behaves as a critical gate

dx.doi.org/10.1021/bi401137u | Biochemistry 2013, 52, 9120−9128

for the entry of FMN into the binding pocket.[37] Thus, the dominant 340 fs component represents the major ET dynamics, and the minor 1.82 ps component probably reflects a loose, unstable configuration. The observation of the single-exponential decay is in contrast to the reported double-exponential decay dynamics for mutants studied by the Mataga group,[28] possibly a question of the freshness of samples used in their reports. Nevertheless, our single-exponential decay dynamics of the mutants are consistent with the major components reported by the Mataga group. For example, our values of 157 fs for the WT, 258 fs for Y98F, and 302 fs for W60F are similar to the reported values of 158 fs (92%), 245 fs (85%), and 322 fs (83%) for the same mutants,[28] respectively.

The obtained dynamics of charge separation are ultrafast in the range of 135−340 fs, and our previously reported active-site relaxation takes >1 ps.[24] Thus, upon initial excitation, the electron transfer is much faster than the local environment relaxation. The ET reaction occurs in a nonequilibrium configuration. On the time scale of electron transfer, the active site appears to be nearly frozen. The concept of reorganization energy (λ) is not be applicable here, and the forward ET reaction mainly depends on the reduction potentials (mainly enthalpy difference) of the donor and acceptor, the driving force of the reaction, similar to the ET reaction in the gas phase that is determined by the donor ionization energy and acceptor electron affinity. The reduction potential of $W^{\bullet+}/W$ is approximately 1.15 V versus the normal hydrogen electrode (NHE)[38] and that of $Y^{\bullet+}/Y$ approximately 1.47 V versus the NHE[39−42] at pH 7. The reduction potentials of FMN/$FMN^{\bullet-}$ can be obtained from those of FMN/$FMNH^{\bullet}$[39] for the different mutants[29,31,43−45] in a range of −0.54 to −0.35 V versus the NHE. Thus, the corresponding FET and BET free energies are also listed in Table 1. Clearly, for case i of Y donor only and case ii of W donor only, the FET is faster for case ii [0.2−0.25 ps ($1/k_2$)] than for case i [0.3−0.34 ps ($1/k_1$)], mainly due to the difference in the reduction potential energies of two Y and W donors. For case iii, the dual Y donors (0.258 ps) are faster than the single Y donor in case i. For case iv, the dual donors of Y and W clearly accelerate the FET reaction, resulting in even faster dynamics of ∼0.15 ps. We did not observe a measurable signal for the dual W donors (W60/W98) with our time resolution; the FET dynamics is probably super ultrafast (<50 fs), or the system upon excitation is already in the charge-separated state due to the charge transfer character in the ground or excited state.[31]

Overall, the observed FET reaction times follow the trend of their driving force changes, but for the fixed donor(s), the FET dynamics have minor variations with mutations in case iv. For mutants G61A and G61V, the large changes in the reduction potentials for FMN/$FMNH^{\bullet}$ ($E_{m,7}$ in Table 1) are due to the second-step protonation process from one-electron reduced $FMN^{\bullet-}$ to $FMNH^{\bullet}$, the key effect of the G61 mutation,[29] and thus, the charge separation for the first-step reduction of FMN/$FMN^{\bullet-}$ would not be significantly affected. Thus, the change in the FET dynamics is mainly from the difference (320 mV) in the reduction potentials of W and Y. The reduction of FMN* to $FMN^{\bullet-}$ depends on the total available aromatic residues (W and/or Y) in the proximity. The Mataga group has recently discussed in detail the ultrafast FET mechanism in flavoproteins using the average distance instead of the edge-to-edge distance between the donor and acceptor.[46,47] However, the usage of solvent reorganization energy (λ) in their discussion is probably not appropriate as we pointed out above, because the ET dynamics are much faster than the active-site relaxation, i.e., the nearly frozen active site on the femtosecond time scale.

Ultrafast Charge Recombination, Hot Product Formation, and Subsequent Vibrational Cooling. Figures 4−6 show the typical absorption transients for four ET cases

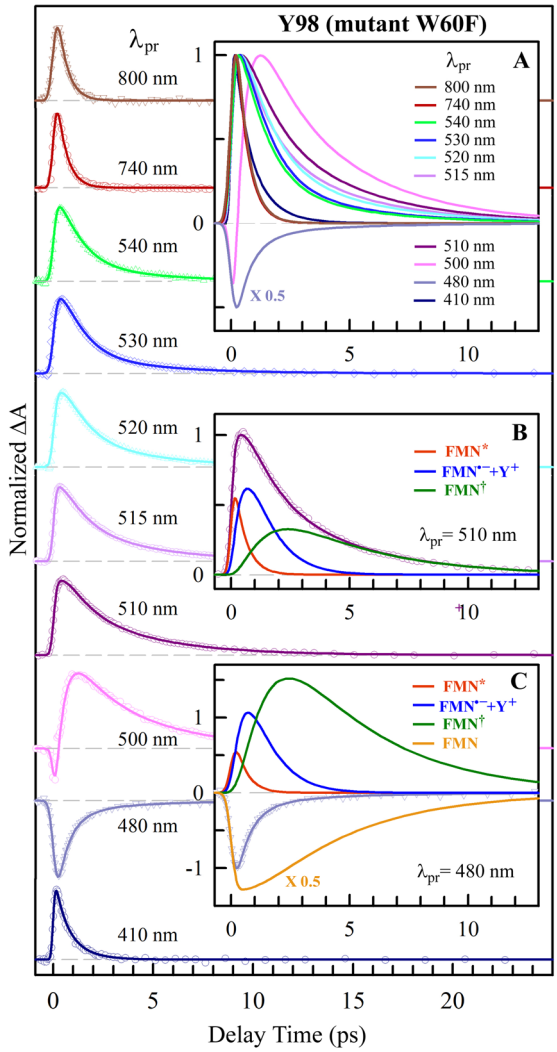

Figure 4. Normalized femtosecond-resolved absorption transients of mutant W60F flavodoxin probed from 800 to 410 nm for the ET reaction 1 with only donor Y98. Inset A shows the entire evolution of the dynamics with probe wavelengths. Insets B and C show the deconvolution of the transients into various species probed at 510 and 480 nm, respectively. Note that at 480 nm the transient becomes faster again as a result of cancellation of ground-state FMN recovery (light orange line) by the positive signal of $FMN^{\dagger}$ (green line).

with a wide range of detection wavelengths from 800 to 400 nm to monitor the dynamics from the reactants (FMN*) to charge-separated intermediates ($FMN^{\bullet-}$ and $Y^{\bullet+}/W^{\bullet+}$) to final products ($FMN^{\dagger}$ and FMN). Specifically, Figure 4 shows the complete ET dynamics of Y98 (W60F mutant) in case i, and Figure 4A shows the entire evolution of the transients. At 800 and 740 nm, both transients are the same, and we detected only the excited reactant FMN*. The dynamics follow a single-exponential decay in 0.49 ps, slower than that from the fluorescence detection (0.3 ps), which seems to be a general phenomenon and was observed in many other systems.[48] The absorption method may sense more donor−acceptor config-

dx.doi.org/10.1021/bi401137u | Biochemistry 2013, 52, 9120−9128

urations than fluorescence detection. When the probe wavelength was tuned to the blue side, the dynamics clearly become slower and the time scales longer (Figure 4A). In particular, when the dynamics were probed at the red side of the ground-state absorption from 540 to 500 nm, the transients become slower and slower. Clearly, if we detected only the excited FMN* and intermediates $FMN^{\bullet-}$ and $Y^{\bullet+}$, the dynamics should not change dramatically even though the percentage of each species could change. Thus, the only possibility is that we observed the dynamics of hot ground-state $FMN^{\dagger}$ after charge recombination (Figure 4B); such vibrationally excited states have their absorptions move to the red side of the original ground-state absorption (Figure 2B). Therefore, we observed a series of hot ground-state relaxation, and the dynamics change from faster to slower as vibrational cooling from higher- to lower-energy states proceeds. At 480 nm, we observed the ground-state recovery and the overall dynamics becomes faster again because of the cancellation of slow cooling contributions by ground-state formation signals (Figure 4C). At 410 nm, we observed the positive signal again from the contributions of the excited FMN* and intermediates $FMN^{\bullet-}$ and $Y^{\bullet+}$. Thus, the global fitting of all these transients gave values of 0.95 ps (k_3^{-1}) for charge recombination and 3.7−4.0 ps (k_5^{-1}) for vibrational relaxation of hot ground states.

The observation of ground-state vibrational excitation after BET in protein flavodoxin is significant. The vibrationally coupled ET through high-frequency modes was observed in BET of several chemical systems.[18,19,49] For the flavodoxin studied here, the BET dynamics (<1 ps) is even faster than the active-site relaxation (≥1 ps), and thus, the active-site motions are only partially coupled with the BET dynamics. With a van der Waals distance of 3.34 Å between the donor tyrosine and acceptor isoalloxazine ring,[22] the formed $FMN^{\bullet-}\cdots Y^{\bullet+}$ ion pair would proceed to vibrational motions as observed in the gas-phase benzene···iodine charge transfer complex.[50] The ultrafast BET, faster than the active-site relaxation, must efficiently channel ionic energy into high-frequency vibrational energy of ground-state FMN (and/or Y), leading to the formation of hot $FMN^{\dagger}$, a molecular picture similar to hot ground-state benzene formation in BET of the benzene···iodine charge transfer complex.[50] Such ultrafast ET reactions in flavodoxin bear some similarity to gas-phase bimolecular charge transfer reactions.[50,51] If we consider the absorption shift from 500 to 540 nm due to hot ground-state formation, a total vibrational energy of ∼1500 cm^{-1} is obtained for hot $FMN^{\dagger}$ with a few vibrational quantum numbers (ν = 1−3), given some high-frequency vibrational modes of FMN in the range of 500−1500 cm^{-1}.[52] The cooling dynamics occur in a few picoseconds, slower than all ET dynamics, and thus allow us to observe the hot $FMN^{\dagger}$ formation and subsequent cooling dynamics. The time scale of 3−4 ps is similar to that of $FMN^{\dagger}$ cooling in polar solvents,[53,54] implying one possibility that the vibrational energy may flow into the water molecules around the entrance of the active site. Such cooling dynamics is also mixed with the active-site relaxation induced by fast charge recombination. Mutant W60A exhibits results similar to those of mutant W60F (see in Table 1).

Figure 5 shows the absorption transients of mutant W60 (Y98F), and a similar dynamic pattern was observed. At longer probing wavelengths of 800−580 nm (insets of A and B of Figure 5), we detected the excited FMN* dynamics in 0.37 ps (k_2^{-1}) as well as the formation and decay dynamics of intermediate $W^{\bullet+}$ in 0.37 and 1.4 ps, respectively. The transient

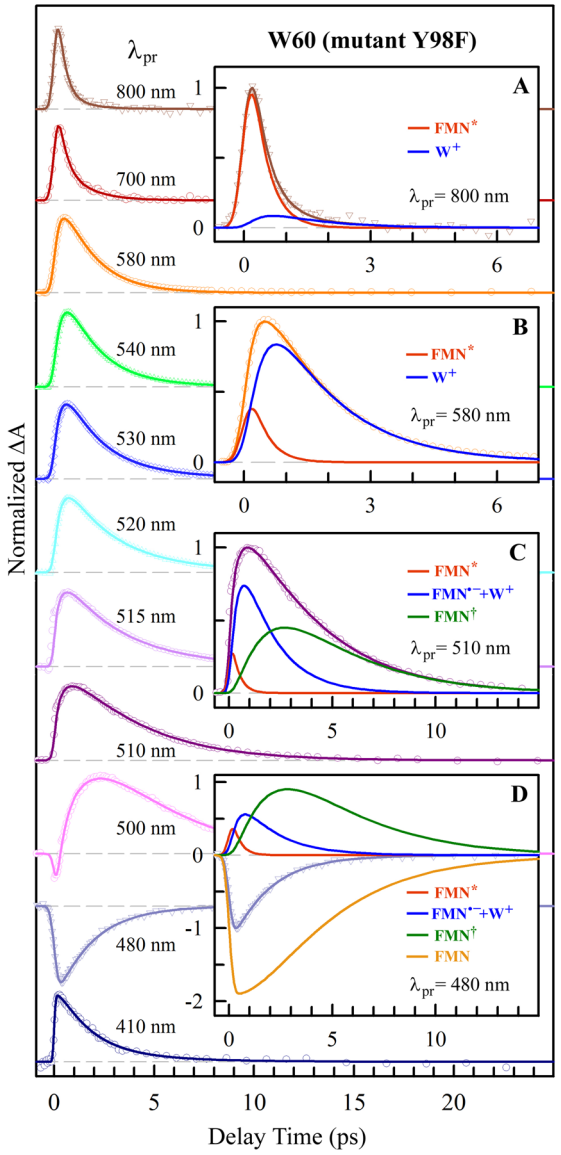

Figure 5. Normalized femtosecond-resolved absorption transients of mutant Y98F flavodoxin probed from 800 to 410 nm for ET reaction 2 with only donor W60. Insets A−D show the deconvolution of the transients into various species probed at 800, 580, 510, and 480 nm, respectively, showing the step-by-step detection of the initial reactant (FMN*), intermediates ($FMN^{\bullet-}$ and $W^{\bullet+}$), and final products ($FMN^{\dagger}$ and FMN). Note that at 480 nm the transient becomes faster again as in Figure 4.

at 580 nm shows the dominant contribution of the intermediate state due to the strong absorption of tryptophan cation $W^{\bullet+}$.[40] Similarly, we observed the vibrational cooling dynamics at wavelengths shorter than 540 nm in 3.3−3.8 ps, similar to that observed in mutant Y98 (W60F). Also, the ground-state recovery transient of the product FMN at 480 nm becomes faster, again because of the cancellation of contributions of the cooling dynamics and relaxed ground-state formation dynamics. For the other mutants in Table 1, we obtained similar time scales with minor changes. Typically, the charge recombination of photoinduced charge separation is in the Marcus inverted region because the free energy of charge recombination is usually larger than the reorganization energy. As shown in Table 1, the BET reaction for W60 has a free energy (−1.54 to −1.50 eV) smaller than that of Y98 (−1.84 eV), but we

dx.doi.org/10.1021/bi401137u | Biochemistry 2013, 52, 9120−9128

observed slower BET dynamics for W60 and faster dynamics for Y98, indicating an unusual behavior given that the reorganization energy for the ET reaction of anionic flavin radical in flavoproteins is usually <1.5 eV.[55,56] This phenomenon must result from the faster BET and slower active-site relaxation.

Figure 6 shows the ET reactions with dual donors Y and W, and overall, a similar pattern was observed with the striking

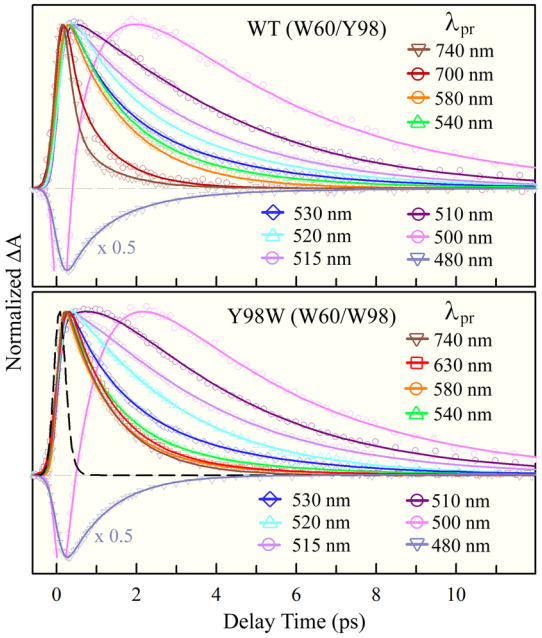

Figure 6. Normalized femtosecond-resolved absorption transients of wild-type flavodoxin (top) for ET reactions 1 and 2 with dual donors W60 and Y98 and the Y98W mutant (bottom) with dual donors W60 and W98 (reaction 2) probed with a series of wavelengths from 740 to 410 nm, showing the striking evolution when the probe wavelength was tuned to the blue side. The black dashed line in the bottom panel shows a simulated 100 fs decay for comparison with a 1.1 ps decay in the 740 nm transient. The negative signals probed at 500 nm are not completely shown here.

vibrational cooling dynamics again. As seen in reactions 1 and 2, for the wild type, we observed ultrafast FET dynamics (k_1 + k_2) mainly at 740 and 700 nm. At 580 nm, we observed the dominant $W^{\bullet+}$ contribution and thus obtained the decay dynamics of BET in 1.56 ps (k_4^{-1}) by reaction 2, similar to the mutant W60 (Y98F) in Figure 5. The overall fitting gave the BET dynamics of reaction 1 in ~0.95 ps for $FMN^{\bullet-}$ + $Y^{\bullet+}$ charge recombination, similar to the single-Y donor BET dynamics. Although we observed a total FET rate from both W and Y, we resolved the individual charge recombination dynamics of Y and W (k_3 and k_4). This observation is important, and we can compare the obtained BET dynamics from two donors with the results from the single donors. Here, we observed similar BET dynamics (k_3 or k_4) for the same donor even for the different initial FET reactions. The cooling dynamics occur in 3.0−4.3 ps. For mutant Y98W, because the absorption shows the charge transfer character (Figure 2) we did not observe any FET dynamics as shown in Figure 6 (bottom panel). At 800 nm, the signal is negligible and is 1−2 orders of magnitude weaker than the signal of the mutant W60 (Y98F) in Figure 5. At 740 nm, the signal is also very weak and represents only the $W^{\bullet+}$ dynamics of charge recombination in 1.1 ps (k_4^{-1}); see the dashed line of a simulated 100 fs decay for comparison. From 630 nm, we started to detect the cooling dynamics (Figure 2) after charge recombination. The transient at 580 nm appears faster than that at 630 nm because of the dominant $W^{\bullet+}$ contribution in the former, and actually, the cooling dynamics is similar around 3 ps (k_S^{-1}) in both transients. The transients at the shorter wavelengths follow a pattern similar to that of other mutants, and the cooling relaxation takes 3−4 ps. All other mutants with the dual donors also have similar dynamics as listed in Table 1.

Photoinduced Redox Cycle, Reaction Time Scales, and Vibrational Coupling Generality. The photoinduced redox cycle at the active site of flavodoxin is given in Figure 7A. Four fundamental processes are involved in the redox cycle, initial forward ET (τ_{FET}), subsequent back ET (τ_{BET}), subsequent vibrational product cooling (τ_C), continuous active-site solvation (τ_S),[24] that was determined in our previous studies. The active-site relaxation evolves with the entire dynamic process from the initial excitation to charge separation to charge recombination and finally to vibrational cooling. The complete solvation at the active site occurs on multiple time scales in 1.0 ps (53%), 25 ps (26%), and 670 ps (21%), involving various motions at the active site, including neighboring hydration water molecules.[24] The 1.0 ps dynamics mainly comes from the initial local relaxation of hydration water networks around the active site at the protein surface.[24,57] Thus, the four time scales involved are critical to our observation and our understanding of the ET molecular mechanism.

For flavodoxin, τ_{FET} is ultrafast and the solvation appears to be frozen, a gas-phase type of bimolecular charge transfer reaction. τ_{BET} is also very fast on a similar time scale of initial solvation. Thus, the BET is a nonequilibrium ET dynamics and theoretically could be treated by the extended Sumi−Marcus two-dimensional model (solvent and nuclear coordinates), leading to a nonexponential behavior typically in a stretched exponential decay. However, we observed the dominant single-exponential decay for BET (such as W^+ decay at 580 nm), indicating that the coupling of BET with solvent relaxation is not severe yet. Because of the stacking nature of the donor and acceptor and the hydrating water molecules not intercalating between the donor and acceptor, the charge-separated complex ($FMN^{\bullet-}\cdots Y^{\bullet+}/W^{\bullet+}$) could have significant intermolecular vibrations and thus lead to high-frequency vibrational excitation of products $FMN^{\dagger}\cdots Y^{\dagger}/W^{\dagger}$, resulting in very fast BET dynamics. However, if τ_{FET} and τ_{BET} are much longer than τ_S, we would also observe a single-exponential decay for both equilibrated ET dynamics with a relaxed active-site configuration. If τ_{FET} or τ_{BET} is longer than τ_C, we would not observe the vibrational cooling process because the rate-determining step would be the longer ET dynamics, and the hot products would not accumulate. Thus, the protein flavodoxin is an ideal model system for directly observing the vibrationally accelerated BET dynamics with all resolved elementary processes in a redox cycle in the active-site environment of the protein.

With the 11 mutants and WT flavodoxin, we resolved all three elementary dynamics of FET, BET, and vibrational cooling as well as active-site solvation dynamics. With the reported redox potentials of FMN in these mutants (Table 1), the ET dynamics mainly follow the redox trend of the donor W or Y but slightly change with the reduction potential of FMN by mutations. For the stacked, compact FMN···Y/W pair, the

dx.doi.org/10.1021/bi401137u | Biochemistry 2013, 52, 9120−9128

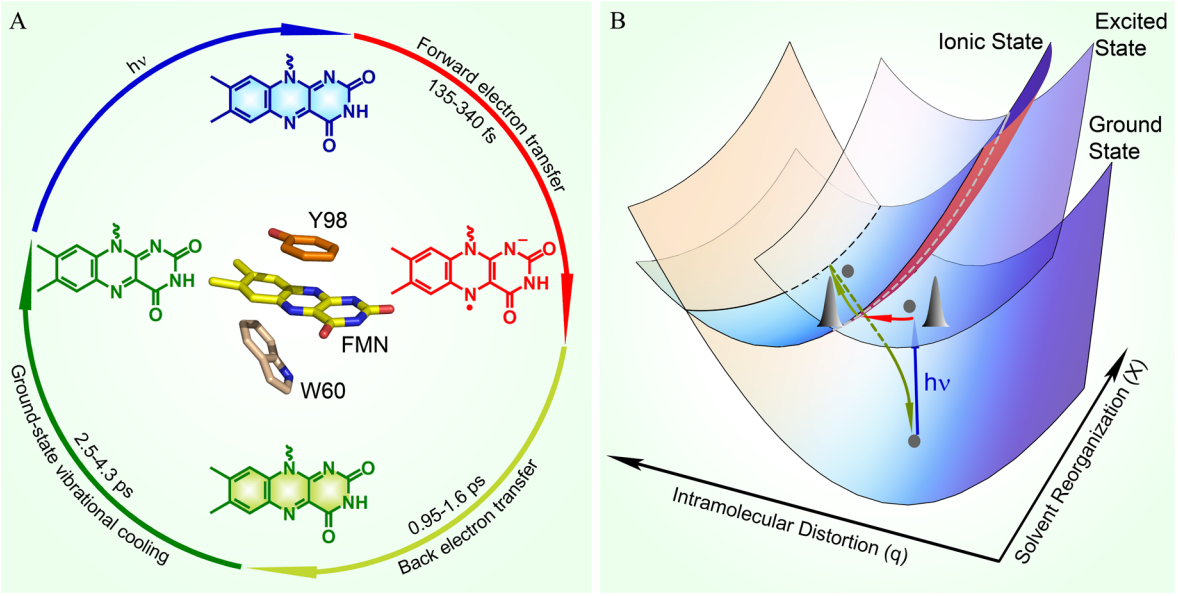

Figure 7. (A) Complete photoinduced redox cycle in flavodoxin with all resolved elementary dynamics and their time scales. The active-site relaxation (not shown) is involved in all these processes on the picosecond time scales. (B) Schematic presentation of the three potential surfaces involved in the photoinduced redox cycle along two coordinates, intramolecular distortion and solvent reorganization. The three dots represent the equilibrium configurations on the three surfaces. The high-frequency ground-state vibrational excitation is not shown during the transition from the ionic state to the ground state.

ET reaction mainly occurs between the donor and acceptor. The environment has a main static effect with a minor dynamic influence. Figure 7B shows the schematic potential surfaces of three states along two coordinates of intramolecular distortion (q) and solvent reorganization (X). The initial FET mainly evolves along the intramolecular nuclear coordinate because of the relatively slow solvation. Thus, the observed deceleration of the FET in the crystal of a similar FMN-binding protein is probably not due to the slow solvation in the crystal[58] because the FET dynamics is much faster than the solvation process, even more so in the crystal. After charge separation, the ionic complex continuously moves along the nuclear coordinate and meanwhile also evolves along the solvation coordinate to reach the minimal crossing seam to the ground-state surface with high-frequency vibrational excitation (not shown in Figure 7B) to conserve the total energy. The molecular picture revealed here should be applicable to many other flavoproteins because of the common structural configurations and interactions between aromatic residues and cofactor flavin. Thus, the vibrational excitation after charge recombination and subsequent cooling dynamics should be general to flavoproteins even though the cooling dynamics could be often buried in the rate-determining slow ET process.

CONCLUSION

We report here our complete characterization of a photoinduced short-range cyclic electron transfer of oxidized flavin (FMN) in the protein flavodoxin. With femtosecond resolution, we can follow the entire redox reactions, forward and backward electron transfer, from the reactants to all intermediates and finally to products (Figure 7A). The forward electron transfer occurs ultrafast with stacked aromatic residue(s) (tryptophan or tyrosine) in 130−350 fs, much faster than the active-site relaxation, which occurs on picosecond time scales. With 11 mutations at the active site, the electron transfer dynamics have minor changes, a reaction highly localized between the donor and acceptor at a van der Waals distance, leading to a gas-phase type of bimolecular reaction confined in the active-site nanospace. The environment exerts an electrostatic effect on the reactions with a minor dynamic influence.

The charge-separated complex evolves along nuclear and solvent coordinates (Figure 7B). Along the nuclear coordinate, the ionic donor−acceptor vibrations strongly couple with the donor−acceptor high-frequency modes. Along the solvent coordinate, the ionic complex couples with the active-site motions of the protein and neighboring hydration water molecules (around the entrance of the active site). As a result, the hot ground-state product(s) was formed with accelerated charge recombination in 1−2 ps. The vibrationally excited product cools in 3−4 ps at the active site, presumably channeling the energy to hydrating water molecules. The faster electron transfer dynamics and slower cooling relaxations allow the direct observation of such a vibrational effect on acceleration of the back electron transfer reaction. The observed vibrational effect should be general to flavoproteins based on their similar configurations and interactions between the cofactor flavin and neighboring aromatic residues at the active sites and should be considered in charge recombination reactions in flavoproteins.

AUTHOR INFORMATION

Corresponding Author

*E-mail: zhong.28@asc.ohio-state.edu. Telephone: (614) 292-3044. Fax: (614) 292-7557.

Author Contributions

T.-F.H. and L.G. contributed equally to this work.

Funding

This work is supported in part by National Institutes of Health Grant GM074813, National Science Foundation Grant CHE0748358, and the Camille Dreyfus Teacher-Scholar award (to D.Z.).

Notes

The authors declare no competing financial interest.

■ ACKNOWLEDGMENTS

We thank Prof. Richard Swenson (The Ohio State University) for the generous gift of the flavodoxin plasmid and helpful discussion. We also thank Zheyun Liu and Chuang Tan for the help with some of the figures and references.

■ REFERENCES

(1) Iwai, M., Takizawa, K., Tokutsu, R., Okamuro, A., and Minagawa, J. (2010) Isolation of the elusive supercomplex that drives cyclic electron flow in photosynthesis. *Nature 464*, 1210−1213.

(2) Wang, H., Lin, S., Allen, J. P., Williams, J. C., Blankert, S., Laser, C., and Woodbury, N. W. (2007) Protein dynamics control the kinetics of initial electron transfer in photosynthesis. *Science 316*, 747−750.

(3) Kao, Y.-T., Saxena, C., Wang, L., Sancar, A., and Zhong, D. (2005) Direct observation of thymine dimer repair in DNA by photolyase. *Proc. Natl. Acad. Sci. U.S.A. 102*, 16128−16132.

(4) Li, J., Liu, Z., Tan, C., Guo, X., Wang, L., Sancar, A., and Zhong, D. (2010) Dynamics and mechanism of repair of ultraviolet-induced (6−4) photoproduct by photolyase. *Nature 466*, 887−890.

(5) Liu, Z., Tan, C., Guo, X., Kao, Y.-T., Li, J., Wang, L., Sancar, A., and Zhong, D. (2011) Dynamics and mechanism of cyclobutane pyrimidine dimer repair by DNA photolyase. *Proc. Natl. Acad. Sci. U.S.A. 108*, 14831−14836.

(6) Gauden, M., van Stokkum, I. H. M., Key, J. M., Lührs, D. Ch., van Grondelle, R., Hegemann, P., and Kennis, J. T. M. (2006) Hydrogen-bond switching through a radical pair mechanism in a flavin-binding photoreceptor. *Proc. Natl. Acad. Sci. U.S.A. 103*, 10895−10900.

(7) Ozturk, N., Selby, C. P., Annayev, Y., Zhong, D., and Sancar, A. (2011) Reaction mechanism of *Drosophila* cryptochrome. *Proc. Natl. Acad. Sci. U.S.A. 108*, 516−521.

(8) Xiong, P., Nocek, J. M., Vura-Weis, J., Lockard, J. V., Wasielewski, M. R., and Hoffman, B. M. (2010) Faster interprotein electron transfer in a [myoglobin, b_5] complex with a redesigned interface. *Science 330*, 1075−1078.

(9) Gray, H. B., and Winkler, J. R. (2005) Long-range electron transfer. *Proc. Natl. Acad. Sci. U.S.A. 102*, 3534−3539.

(10) Stubbe, J., Nocera, D. G., Yee, C. S., and Chang, M. C. Y. (2003) Radical initiation in the class I ribonucleotide reductase: Long-range proton-coupled electron transfer? *Chem. Rev. 103*, 2167−2201.

(11) Page, C. C., Moser, C. C., Chen, X. X., and Dutton, P. L. (1999) Natural engineering principles of electron tunnelling in biological oxidation-reduction. *Nature 402*, 47−52.

(12) Daizadeh, I., Medvedev, E. S., and Stuchebrukhov, A. A. (1997) Effect of protein dynamics on biological electron transfer. *Proc. Natl. Acad. Sci. U.S.A. 94*, 3703−3708.

(13) Lin, J. P., Balabin, I. A., and Beratan, D. N. (2005) The nature of aqueous tunneling pathways between electron-transfer proteins. *Science 310*, 1311−1313.

(14) Berlin, Y. A., Burin, A. L., Siebbeles, L. D. A., and Ratner, M. A. (2001) Conformationally gated rate processes in biological macromolecules. *J. Phys. Chem. A 105*, 5666−5678.

(15) (a) Warshel, A., and Parson, W. W. (1991) Computer simulations of electron-transfer reactions in solution and in photosynthetic reaction centers. *Annu. Rev. Phys. Chem. 42*, 279−309. (b) Marcus, R. A., and Sutin, N. (1985) Electron transfers in chemistry and biology. *Biochim. Biophys. Acta 811*, 265−322.

(16) Liu, Z., Guo, X., Tan, C., Li, J., Kao, Y.-T., Wang, L., Sancar, A., and Zhong, D. (2012) Electron tunneling pathways and role of adenine in repair of cyclobutane pyrimidine dimer by DNA Photolyase. *J. Am. Chem. Soc. 134*, 8104−8114.

(17) Sumi, H., and Marcus, R. A. (1986) Dynamical effects in electron transfer reactions. *J. Chem. Phys. 84*, 4894−4914.

(18) Walker, G. C., Akesson, E., Johnson, A. E., Levinger, N. E., and Barbara, P. F. (1992) Interplay of solvent motion and vibrational excitation in electron-transfer kinetics: Experiment and theory. *J. Phys. Chem. 96*, 3728−3736.

(19) Nagasawa, Y., Yartsev, A. P., Tominaga, K., Bisht, P. B., Johnson, A. E., and Yoshihara, K. (1995) Dynamical aspects of ultrafast intermolecular electron transfer faster than solvation process: Substituent effects and energy gap dependence. *J. Phys. Chem. 99*, 653−662.

(20) Novoderezhkin, V. I., Yakovlev, A. G., van Grondelle, R., and Shuvalov, V. A. (2004) Coherent nuclear and electronic dynamics in primary charge separation in photosynthetic reactions centers: A redfield theory approach. *J. Phys. Chem. B 108*, 7445−7457.

(21) Kao, Y.-T., Guo, X., Yang, Y., Liu, Z., Hassanali, A., Song, Q.-H., Wang, L., and Zhong, D. (2012) Ultrafast dynamics of nonequilibrium electron transfer in photoinduced redox cycle: Solvent mediation and conformation flexibility. *J. Phys. Chem. B 116*, 9130−9140.

(22) Sancho, J. (2006) Flavodoxins: Sequence, folding, binding, function and beyond. *Cell. Mol. Life Sci. 63*, 855−864.

(23) Watt, W., Tulinsky, A., Swenson, R. P., and Watenpaugh, K. D. (1991) Comparison of the crystal structures of a flavodoxin in its three oxidation states at cryogenic temperatures. *J. Mol. Biol. 218*, 195−208.

(24) Chang, C.-W., He, T.-F., Guo, L., Stevens, J. A., Li, T., Wang, L., and Zhong, D. (2010) Mapping solvation dynamics at the function site of flavodoxin in three redox states. *J. Am. Chem. Soc. 132*, 12741−12747.

(25) Zhong, D., and Zewail, A. H. (2001) Femtosecond dynamics of flavoproteins: Charge separation and recombination in riboflavine (vitamin B_2)-binding protein and in glucose oxidase enzyme. *Proc. Natl. Acad. Sci. U.S.A. 98*, 11867−11872.

(26) Pan, J., Byrdin, M., Aubert, C., Eker, A. P. M., Brettel, K., and Vos, M. H. (2004) Excited-state properties of flavin radicals in flavoproteins: Femtosecond spectroscopy of DNA photolyase, glucose oxidase, and flavodoxin. *J. Phys. Chem. B 108*, 10160−10167.

(27) Kao, Y.-T., Tan, C., Song, S.-H., Oztürk, N., Li, J., Wang, L., Sancar, A., and Zhong, D. (2008) Ultrafast dynamics and anionic active states of the flavin cofactor in cryptochrome and photolyase. *J. Am. Chem. Soc. 130*, 7695−7701.

(28) Mataga, N., Chosrowjan, H., Taniguchi, S., Tanaka, F., Kido, N., and Kitamura, M. (2002) Femtosecond fluorescence dynamics of flavoproteins: Comparative studies on flavodoxin, its site-directed mutants, and riboflavin binding protein regarding ultrafast electron transfer in protein nanospaces. *J. Phys. Chem. B 106*, 8917−8920.

(29) O'Farrell, P. A., Walsh, M. A., McCarthy, A. A., Higgins, T. M., Voordouw, G., and Mayhew, S. G. (1998) Modulation of the redox potentials of FMN in *Desulfovibrio vulgaris* flavodoxin: Thermodynamic properties and crystal structures of glycine-61 mutants. *Biochemistry 37*, 8405−8416.

(30) Zhou, Z., and Swenson, R. P. (1995) Electrostatic effects of surface acidic amino acid residues on the oxidation-reduction potentials of the flavodoxin from *Desulfovibrio vulgaris* (Hildenborough). *Biochemistry 34*, 3183−3192.

(31) Swenson, R. P., and Krey, G. D. (1994) Site-directed mutagenesis of tyrosine-98 in the flavodoxin from *Desulfovibrio vulgaris* (Hildenborough): Regulation of oxidation-reduction properties of the bound FMN cofactor by aromatic, solvent, and electrostatic interactions. *Biochemistry 33*, 8505−8514.

(32) Mayhew, S. G., and Massey, V. (1969) Purification and characterization of flavodoxin from *Peptostreptococcus elsdenii*. *J. Biol. Chem. 244*, 794−802.

(33) Chaitanya, S., Sancar, A., and Zhong, D. (2004) Femtosecond dynamics of DNA photolyase: Energy transfer of antenna initiation and electron transfer of cofactor reduction. *J. Phys. Chem. B 108*, 18026−18033.

(34) Karen, A., Sawada, M. T., Tanaka, F., and Mataga, N. (1987) Dynamics of excited flavoproteins: Picosecond laser photolysis studies. *Photochem. Photobiol. 45*, 49−53.

(35) Edmondson, D. E., and Tollin, G. (1983) Semiquinone formation in flavo- and metalloflavoproteins. *Top. Curr. Chem. 108*, 109−138.

(36) Ganapathi, M. R., Hermann, R., Naumov, S., and Brede, O. (2000) Free electron transfer from several phenols to radical cations of non-polar solvents. *Phys. Chem. Chem. Phys. 2*, 4947−4955.
(37) Genzor, C. G., Operales-Alcon, A., Sancho, J., and Romero, A. (1996) Closure of a tyrosine/tryptophan aromatic gate leads to a compact fold in apo flavodoxin. *Nat. Struct. Biol. 3*, 329−332.
(38) DeFelippis, M. R., Murthy, C. P., Klapper, M. H., Broitman, F., Weinraub, D., and Faraggi, M. (1991) Electrochemical properties of tyrosine phenoxy and tryptophan indolyl radicals in peptides and amino acid analogues. *J. Phys. Chem. 95*, 3416−3419.
(39) Dutton, P. L. (1978) Redox potentiometry: Determination of midpoint potentials of oxidation-reduction components of biological electron-transfer systems. *Methods Enzymol. 54*, 411−435.
(40) Dixon, W. T., and Murphy, D. (1976) Determination of the acidity constants of some phenol radical cations by means of electron spin resonance. *J. Chem. Soc., Faraday Trans. 72*, 1221−1230.
(41) Tommos, C., Skalicky, J. J., Pilloud, D. L., Wand, A. J., and Dutton, P. L. (1999) De novo proteins as models of radical enzyme. *Biochemistry 38*, 9495−9507.
(42) Harriman, A. (1987) Further comments on the redox potentials of tryptophan and tyrosine. *J. Phys. Chem. 91*, 6102−6104.
(43) Mayhew, S. G., O'Connel, D. P., O'Farrell, P. A., Yalloway, G. N., and Geoghegan, S. M. (1996) Regulation of the redox potentials of flavodoxins: Modification of the flavin binding site. *Biochem. Soc. Trans. 24*, 122−127.
(44) McCarthy, A. A., Walsh, M. A., Verma, C. S., O'Connell, D. P., Reinhold, M., Yalloway, G. N., D'Arcy, D., Higgins, T. M., Voordouw, G., and Mayhew, S. G. (2002) Crystallographic investigation of the role of aspartate 95 in the modulation of the redox potentials of *Desulfovibrio vulgaris* flavodoxin. *Biochemistry 41*, 10950−10962.
(45) Edwards, A. M. (2006) General properties of flavins. In *Flavins: Photochemistry and photobiology* (Silva, E., and Edwards, A. M., Eds.) pp 1−11, Royal Society of Chemistry, Cambridge, U.K.
(46) Nunthaboot, N., Tanaka, F., Kokpol, S., Chosrowjan, H., Taniguchi, S., and Mataga, N. (2008) Simultaneous analysis of ultrafast fluorescence decays of FMN binding protein and its mutated proteins by molecular dynamic simulation and electron transfer Theory. *J. Phys. Chem. B 112*, 13121−13127.
(47) Lugsanangarm, K., Pianwanit, S., Kokpol, S., Tanaka, F., Chosrowjan, H., Taniguchi, S., and Mataga, N. (2011) Photoinduced electron transfer in wild type and mutated flavodoxin from *Desulfovibrio vulgaris*, strain Miyazaki F.: Energy gap law. *J. Photochem. Photobiol., A 219*, 32−41.
(48) Wan, C., Xia, T., Becker, H.-C., and Zewail, A. H. (2005) Ultrafast unequilibrated charge transfer: A new channel in the quenching of fluorescent biological Probes. *Chem. Phys. Lett. 412*, 158−163.
(49) Gladkikh, V., Burshtein, A. I., Feskov, S. V., Ivanov, A. I., and Vauthey, E. (2005) Hot recombination of photogenerated ion pairs. *J. Chem. Phys. 123*, 244510.
(50) Cheng, P. Y., Zhong, D., and Zewail, A. H. (1996) Femtosecond real-time probing of reactions. XXI. Direct observation of transition-state dynamics and structure in charge-transfer reactions. *J. Chem. Phys. 105*, 6216−6248.
(51) Zhong, D., Bernhardt, T. M., and Zewail, A. H. (1999) Femtosecond real-time probing of reactions. 24. Time, velocity, and orientation mapping of the dynamics of dative bonding in bimolecular electron transfer reacctions. *J. Phys. Chem. A 103*, 10093−10117.
(52) Eisenberg, A. S., and Schelvis, J. P. M. (2008) Contributions of the 8-methyl group to the vibrational normal modes of flavin mononucleotide and its 5-methyl semiquinone radical. *J. Phys. Chem. A 112*, 6179−6189.
(53) Wolf, M. M. N., Schumann, C., Gross, R., Domratcheva, T., and Diller, R. (2008) Ultrafast infrared spectroscopy of riboflavin: Dynamics, electronic structure, and vibrational mode analysis. *J. Phys. Chem. B 112*, 13424−13432.
(54) Gil, M., Wang, Y., and Douhal, A. (2012) Ultrafast dynamics of lumichrome in solution and in chemical and biological caging media. *J. Photochem. Photobiol., A 234*, 146−155.
(55) Liu, Z., Tan, C., Guo, X., Li, J., Wang, L., Sancar, A., and Zhong, D. (2013) Determining complete electron flow in the cofactor photoreduction of oxidized photolyase. *Proc. Natl. Acad. Sci. U.S.A. 110*, 12966−12971.
(56) Liu, Z., Zhang, M., Guo, X., Tan, C., Li, J., Wang, L., Sancar, A., and Zhong, D. (2013) Dynamic determination of the functional state in photolyase and the implication for cryptochrome. *Proc. Natl. Acad. Sci. U.S.A. 110*, 12972−12977.
(57) Zhong, D. (2009) Hydration dynamics and coupled water-protein fluctuations probed by intrinsic tryptophan. *Adv. Chem. Phys. 143*, 83−149.
(58) Chosrowjan, H., Taniguchi, S., Mataga, N., Tanaka, F., Todoroki, D., and Kitamura, M. (2007) Comparison between ultrafast fluorescence dynamics of FMN binding protein from *Desulfovibrio vulgaris*, strain Miyazaki, in solution vs crystal phases. *J. Phys. Chem. B 111*, 8695−8697.